Original Article

Anatomical location-related hemodynamic variations are associated with atherosclerosis in the middle cerebral artery: a preliminary cross-sectional 4D flow and 3D vessel wall MRI study

Peirong Jiang[1]^, Lixin Liu[2], Huiyu Qiao[3], Xiuzhu Xu[1], Yanping Zheng[1], Lin Lin[1], Jialin Chen[4], Bin Sun[1], He Wang[2,5], Xihai Zhao[6], Zhensen Chen[2,5], Yunjing Xue[1]

[1]Department of Radiology, Fujian Medical University Union Hospital, Fuzhou, China; [2]Institute of Science and Technology for Brain-inspired Intelligence, Fudan University, Shanghai, China; [3]School of Biomedical Engineering, Capital Medical University, Beijing, China; [4]Department of Neurology, Fujian Medical University Union Hospital, Fuzhou, China; [5]Key Laboratory of Computational Neuroscience and Brain-Inspired Intelligence (Fudan University), Ministry of Education, Shanghai, China; [6]Center for Biomedical Imaging Research, Department of Biomedical Engineering, School of Medicine, Tsinghua University, Beijing, China

Contributions: (I) Conception and design: P Jiang, Y Xue, Z Chen; (II) Administrative support: Y Xue, Z Chen, H Wang, X Zhao; (III) Provision of study materials or patients: Y Xue, P Jiang, J Chen; (IV) Collection and assembly of data: P Jiang, L Liu, X Xu, Y Zheng, J Chen, B Sun; (V) Data analysis and interpretation: P Jiang, L Liu, H Qiao, Z Chen, X Xu, Y Zheng, L Lin, Y Xue; (VI) Manuscript writing: All authors; (VII) Final approval of manuscript: All authors.

Correspondence to: Yunjing Xue, MD. Department of Radiology, Fujian Medical University Union Hospital, 29 Xinquan Road, Fuzhou 350001, China. Email: xueyunjing@126.com; Zhensen Chen, PhD. Institute of Science and Technology for Brain-inspired Intelligence, Fudan University, 220 Handan Road, Shanghai 200433, China; Key Laboratory of Computational Neuroscience and Brain-Inspired Intelligence (Fudan University), Ministry of Education, 220 Handan Road, Shanghai 200433, China. Email: zhensenchen@163.com.

Background: Hemodynamics is crucial for the assessment of atherosclerotic development. However, flow alterations due to plaque existence and increased plaque number in different intracranial arterial segments have not been fully understood. This study aimed to investigate the relationship of wall shear stress (WSS) parameters between middle cerebral arteries (MCAs) with and without plaque and explore the potential discrepancy between multiple- and single-plaque existence.

Methods: Consecutive patients with MCA atherosclerosis were recruited and underwent four-dimensional (4D) flow magnetic resonance imaging (MRI) and three-dimensional (3D) vessel wall imaging (VWI). Time-averaged WSS (TAWSS), time-averaged WSS coefficient variation (TAWSSCV), and oscillatory shear index (OSI) were measured at five cross-sectional slices [initial, upstream, the most narrowed lumen (MNL), downstream, and terminal] of plaque and reference (REF) sites to describe lesion-level hemodynamics. Segment-level hemodynamics of M1 and M2 segments were also analyzed. MCA geometry and plaque characteristics were calculated. The MCAs were then classified into four groups according to plaque presence in different segments: Group I, without plaque; Group II, with plaque only in M1; Group III, with plaque in both M1 and M2; Group IV, with plaque only in M2. The above parameters were compared in MCA with and without plaque as well as single- and multiple-plaque (≥2) MCAs.

Results: A total of 150 MCAs with 231 plaques from 79 patients were investigated. $TAWSS_{min}$ showed a relatively larger value at the proximal portion compared to the distal portion across plaque in both M1 and M2 segments. Lower lesion-level $TAWSS_{min}$ was found in the M1 plaque presence of Group III compared to Group I and Group II (P=0.026 and P=0.014). Similar association was also observed in the M2 plaque presence of Groups III and IV compared to Group I (P=0.010 and P=0.008), whereas lower segment-level

^ ORCID: 0000-0002-6379-8027.

$TAWSS_{min}$ was only seen in the M2 segment of Group III compared to Group I (P=0.039). Lower OSI_{mean} was found both in the M1 presence of Group II and III compared to Group I (P=0.013 and P=0.048) and OSI_{max} was found in the M1 plaque presence of Group II compared to Group I (P=0.036). Lower stenosis was found in single-plaque compared to multiple-plaque groups (P=0.045 and P=0.049). Lower lesion-level highest/initial $TAWSS_{mean}$ ratio (P=0.037) and highest/initial $TAWSS_{max}$ ratio (P=0.013) were found in the single-plaque M1 group compared to the multiple-plaque M1 group. The M1 geometry and positive remodeling (PR) were different between single- and multiple-plaque M1 groups whereas maximum wall thickness (maxWT) and normalized wall index (NWI) showed differences between the single- and multiple-plaque M2 groups (all P<0.05).

Conclusions: Hemodynamic alterations are observed under the impacts of atherosclerosis and are different between M1 plaque and M2 plaque. Single- and multiple-plaque MCAs exhibit different geometry, plaque characteristics, and hemodynamics, and these vary according to segments. The interplay of arterial segment, plaque number, and characteristics as well as hemodynamics could provide insight for the mechanisms of atherosclerotic existence.

Keywords: Four-dimensional flow magnetic resonance imaging (4D flow MRI); three-dimensional vessel wall imaging (3D VWI); wall shear stress (WSS); atherosclerosis; middle cerebral artery (MCA)

Submitted Oct 01, 2024. Accepted for publication Feb 27, 2025. Published online Mar 13, 2025.
doi: 10.21037/qims-24-1733
View this article at: https://dx.doi.org/10.21037/qims-24-1733

Introduction

Intracranial atherosclerosis (ICAS), especially in the middle cerebral artery (MCA), is commonly observed in patients with ischemic stroke (IS) (1-3). The primary mechanisms of IS involve hemodynamic changes caused by plaque and subsequent lumen stenosis as well as plaque rupture (4-6). Although the entire vascular tree is exposed to the same atherogenic effect of systemic risk factors, previous studies have shown that low wall shear stress (WSS) and high oscillatory shear index (OSI) tend to favor atherogenesis and progression (7-9). The existence of plaque could alter the local WSS topography (10,11). Low WSS and the existence of atherosclerosis have been reported in the human aorta (11), coronary artery (12) and carotid artery (13). However, the relation between OSI and atherosclerosis existence has remained controversial (11,14-17), with some studies having indicated an association between high OSI and plaque existence (9,14,15,17), yet another study having found no such correlation (11). Moreover, previous studies have shown the roles of both oscillatory and non-oscillatory WSS in the development of coronary atherosclerosis (18) as well as both high and low OSI in the development of carotid atherosclerosis (19). Even in the same vascular location, WSS changes over time in response to several systemic and local factors (20) and under the influences of atherosclerosis. For example, vessel geometry (8), the remodeling response of the wall to plaque (20,21), and plaque number (22-26) can critically influence local WSS environment. Identification of such flow parameters and the presence of atherosclerosis would help risk stratification and facilitate optimization clinical prevention. It is therefore of great significance to clarify the relationship between the characteristics of hemodynamics and plaque in atherosclerotic MCA.

Previous studies of the associations between regional hemodynamics and ICAS have mainly been performed for ICAS with moderate-to-severe stenosis (2,5,27) and at the M1 segment of the MCA (5). However, three-dimensional (3D) vessel wall imaging (VWI) has suggested that ICAS with mild stenosis has a potential risk of causing symptoms (28), implying the need for exploration of its hemodynamic impacts (29), which remain underinvestigated (29,30). Despite optimal medical treatment, there remains a risk of IS reoccurrence, leading to a need for further examination of the underlying pathogenesis, especially for mild stenosis (31). Meanwhile, it is well-recognized that high-grade stenosis (e.g., ≥50%) would cause significant perturbation to the regional hemodynamics (32), which becomes an unwanted confounding effect when studying the relationship between hemodynamics and initiation

and development of atherosclerosis. This effect would be mitigated in mild stenosis. Therefore, it is necessary to explore the hemodynamics of ICAS with mild stenosis to gain insight into its pathological significance. Meanwhile, given that different cerebrovascular segments, for example, M1 and M2 segments of MCA, are likely to have different local flow rates, resulting in various hemodynamic conditions, it is important to study whether the plaques located in different segments show similar hemodynamic changes (30). There have been few studies of atherosclerosis and hemodynamics focusing on M2 segments.

Previous studies have elucidated that plaque burden, which can be measured through intracranial or coronary plaque number, is considered a risk factor for stroke recurrence or myocardial infarction (23-26). However, increased plaque number of a single intracranial artery has seldomly been investigated and may be of potential importance for outcome prediction. Therefore, it is vital to explore whether the hemodynamics are different between the single- and multiple-plaque scenarios within the entire MCA.

The impacts of intracranial hemodynamics for IS have been investigated mainly through computational fluid dynamics (CFD) (27,33). However, CFD usually employs a hypothetical inlet flow for all cases, thus does not address the effect of the global flow conditions, such as cardiac output, of each individual. In addition, most intracranial CFD studies only include several large-sized arterial branches and therefore do not consider the influence of the arteries far away from the simulated arteries and the complicated topology of the cerebrovascular network. Therefore, the hemodynamic parameters measured from CFD may have a large difference from the true values. Four-dimensional (4D) flow magnetic resonance imaging (MRI) is a well-validated imaging technique that can measure voxel-wise velocity at multiple cardiac phases (34-36). Previous studies have used 4D flow MRI to explore hemodynamic alterations and distributions in carotid plaque (13) and normal curved M1 segment (8). Time-averaged WSS (TAWSS), time-averaged WSS coefficient variation (TAWSSCV), and OSI can be reliably calculated from 4D flow MRI (8).

Therefore, this study aimed to depict the TAWSS and OSI in MCA with and without plaque and further investigate geometric, plaque, and hemodynamic characteristics between single- and multiple-plaque MCAs in an IS cohort using 4D flow MRI and 3D VWI. We present this article in accordance with the STROBE reporting checklist (available at https://qims.amegroups.com/article/view/10.21037/qims-24-1733/rc).

Methods

Study population

This study was conducted in accordance with the Declaration of Helsinki (as revised in 2013) and approved by the Ethics Committee of Fujian Medical University Union Hospital (No. 2021KJT066). Informed consent was provided by all patients. IS patients with atherosclerotic MCA were enrolled from June 2021 to November 2022 at Fujian Medical University Union Hospital and underwent routine head MRI, 3D time-of-flight (TOF) magnetic resonance angiography (MRA), 3D whole brain black-blood high-resolution VWI (HR-VWI), and 4D flow scans. The inclusion criteria were as follows: (I) age ≥18 years; (II) within 2 weeks of symptom onset; (III) MCA atherosclerosis on the ipsilateral side of the infarction if infarct existed; and (IV) no contraindications to MRI. The exclusion criteria were as follows: (I) non-atherosclerotic vasculopathy (e.g., aneurysm, vasculitis, dissection, arteriovenous malformation, or moyamoya disease); (II) previous intracranial surgery; (III) carotid artery stenosis (≥50%) indicated by vascular imaging examination; (IV) occlusion of MCA; (V) stroke caused by other determined etiology or evidence of cardioembolism on echocardiography or electrocardiogram, such as intracardiac thrombus, intracardiac vegetation, and atrial fibrillation; (VI) prior interventional or surgical treatment of intracranial or extracranial arteries; and (VII) poor image quality.

Demographics (age, sex, and body mass index) and clinical information (current smoking, hypertension, diabetes, hyperlipidemia, coronary disease, prior stroke/transient IS history, and blood pressure at admission) were collected. The National Institutes of Health Stroke Scale (NIHSS) score was evaluated at admission and discharge.

MRI protocols

All magnetic resonance (MR) images were acquired with a 3.0-T MRI scanner (Ingenia CX, Philips Healthcare, Best, the Netherlands) with a 32-channel head coil. The parameters for 3D TOF MRA, 3D HR-VWI, and 4D flow are shown in *Table 1*.

Image interpretation

3D TOF MRA, T1-weighted-volumetric isotropic turbo

Table 1 Parameters of 3D TOF MRA, 3D T1W-VISTA, and 4D flow imaging sequences

Parameters	3D TOF MRA	3D T1W-VISTA	4D flow
TR/TE (ms)	22/3.5	800/20	8.1/3.8
FOV (mm^3)	220×192×106	230×180×180	160×160×35
Voxel size (mm^3)	0.52×0.72×1.2	0.6×0.6×0.6	1×1×1.25
FA (°)	18	90	20
Encoding velocity (cm/s)	–	–	120
Reconstructed cardiac phase	–	–	17

3D, three-dimensional; 4D, four-dimensional; FA, flip angle; FOV, field of view; MRA, magnetic resonance angiography; TE, echo time; T1W-VISTA, T1-weighted-volumetric isotropic turbo spin echo acquisition; TOF, time-of-flight; TR, repetition time.

spin echo acquisition (T1W-VISTA), and 4D flow of each patient were co-registered using the registration tool in the SPM12 toolbox (https://www.fil.ion.ucl.ac.uk/spm/software/spm12/). The intracranial arteries on 3D TOF MRA were automatically segmented using a level-set-based segmentation method and then manually corrected in 3D Slicer (https://www.slicer.org/). M1 segment was defined as the arterial segment between the internal carotid artery bifurcation and the first major MCA bifurcation, whereas the arterial segments after the first major MCA bifurcation to the next major bifurcations were labeled as M2 segments. The more distal segments of MCA and small branches such as lenticulostriate arteries and anterior temporal artery were not included due to the difficulties in achieving reliable 4D flow imaging for the arteries with small diameters.

Atherosclerotic plaques were manually identified through RadiAnt Dicom viewer (https://www.radiantviewer.com/) using T1W-VISTA images by a radiologist with >7 years of experience in vascular imaging. An atherosclerotic plaque was identified as focal vessel wall thickening compared to adjacent proximal, distal, or contralateral vessel segments (37). The multiple plaques were defined as two or more than two plaques in the entire MCA regardless of its located segments. Multiple plaques could be on the same arterial segment or on the different segments, and the determination of multiple plaques was as follows: two plaques were considered as two separate plaques if they were discontinuous and had a normal arterial wall between them. The plaque that involved two segments was considered a single plaque of a segment where the narrowest slice was located. The cross-sectional T1W-VISTA images, perpendicular to the arterial centerline, were generated. Then, the luminal and vessel wall contours of plaques were manually depicted using a custom-developed Matlab tool (38) blinded to the diffusion-weighted imaging results and clinical information. The quantifications of plaque characteristics were calculated as follows: plaque length, maximum wall thickness (maxWT), lumen area (LA), and wall area (WA) at each 1 mm slice, vessel area (VA) as the sum of LA and WA, the degree of stenosis {i.e., [1 – LA at the most narrowed lumen (MNL) slice/LA at the reference (REF) slice] × 100%}, normalized wall index (NWI; WA_{MNL}/VA_{MNL}), and remodeling index (RI; VA_{MNL}/VA_{REF}). The maxWT and WA at the MNL slice were used in the study. The REF slice was defined as the closest normal MCA slice proximal to the plaque at the same segment, and if there was no such normal proximal slice then the closest distal normal slice at the same segment was used instead. Positive remodeling (PR) and negative remodeling (NR) were defined as RI ≥1.05 and RI ≤0.95, and non-remodeling was defined as 0.95< RI <1.05 (2). All patients' M1 segments of MCAs were divided into three geometric types: C type, S type, and line type (39,40). The M1 segment was divided equally into proximal, middle, and distal parts, whereas the M2 segment was divided equally into proximal and distal parts for analysis of plaque distributions. The MCAs were then classified into four groups according to plaque presence in different segments: Group I, without plaque; Group II, with plaque only in M1; Group III, with plaque in both M1 and M2; Group IV, with plaque only in M2. The comparisons of hemodynamics in the presence of M1 plaque (Groups I, II, and III) and M2 plaque (Groups I, III, and IV) were conducted in three groups, respectively. The atherosclerotic MCAs were further classified into single- and multiple-plaque M1 groups as well as single- and multiple-plaque M2 groups for comparisons. In segments with multiple plaques, the most stenotic plaque was used

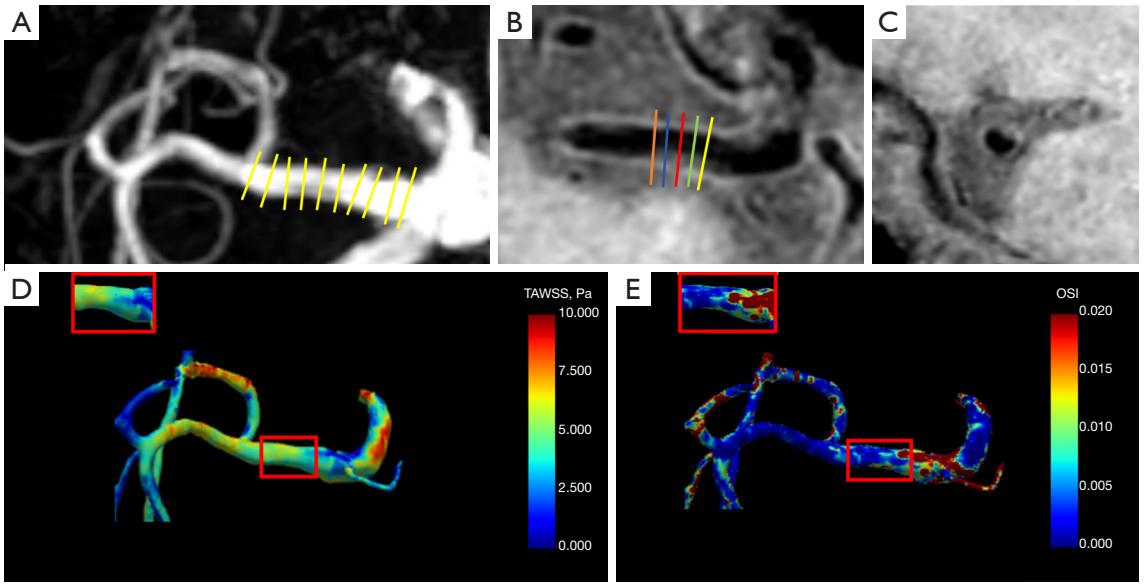

Figure 1 Plaque and hemodynamic measurements of a mild stenotic right MCA. (A) The axial MIP images of 3D TOF MRA with yellow lines indicating slices with 1 mm intervals to calculate segment-level hemodynamics. (B,C) The coronal and cross-sectional MPR images of 3D HR-VWI show five slices across plaque to generate plaque and lesion-level hemodynamic characteristics. Yellow line, initial slice; green line, upstream slice; red line, MNL slice; blue line, downstream slice; orange line, terminal slice. (C) The cross-sectional image of red slice in (B). (D,E) TAWSS and OSI distribution maps. The red boxes in the distribution maps indicate the regional TAWSS and OSI of M1 plaque in (B). The red boxes in the upper right corner show the maps of regional TAWSS and OSI in different orientations. 3D, three-dimensional; HR-VWI, high-resolution vessel wall imaging; MCA, middle cerebral artery; MIP, maximum intensity projection; MNL, the most narrowed lumen; MPR, multiplanar reformation; MRA, magnetic resonance angiography; OSI, oscillatory shear index; TAWSS, time-averaged wall shear stress; TOF, time-of-flight.

when calculating lesion-level plaque characteristics and hemodynamic parameters.

The TAWSS and OSI were calculated from the 4D flow images based on the open-source package (https://github.com/EdwardFerdian/wss_mri_calculator) used in a prior study (41). The input was the segmentation mask from 3D TOF MRA and the velocity fields from 4D flow. Six WSS-derived parameters, including $TAWSS_{mean}$, $TAWSS_{max}$, $TAWSS_{min}$, TAWSSCV, OSI_{mean}, and OSI_{max} over the different locations of the cross-sectional slice were calculated (8). The segment-level hemodynamics were defined as the average hemodynamics of all the cross-sectional slices along the arterial centerlines, with an interval of 1 mm, in specific MCA segments (*Figure 1*). The lesion-level parameters were measured along the plaque at five cross-sectional slices which were perpendicular to the lumen: initial, upstream, MNL, downstream, and terminal (5). The upstream and downstream slices were defined as the middle slices located between the initial or terminal slice and the narrowest slice (5), respectively (*Figure 1*). The above parameters were also counted at the REF slice. Meanwhile, the variability of the TAWSS along the plaque was evaluated as the ratio of the lowest/highest TAWSS slice to the initial slice, as well as the TAWSS ratio of TAWSS at the MNL slice to TAWSS at the REF slice. In Group I, segment-level WSS-derived parameters were used as lesion-level hemodynamic parameters.

Interobserver and intraobserver as well as scan-rescan consistency analysis

Observer 1 and Observer 2 separately analyzed the plaque characteristics and hemodynamic parameters of 20 randomly selected MCAs to assess interobserver and intraobserver consistency. Observer 1 reanalyzed the 20 MCAs 1 month after the initial analysis. In addition, seven healthy volunteers with 14 bilateral MCAs were recruited to perform scan-rescan MRIs of T1W-VISTA, 3D TOF MRA, and 4D flow sequences with an interval of 60 minutes between the two scans.

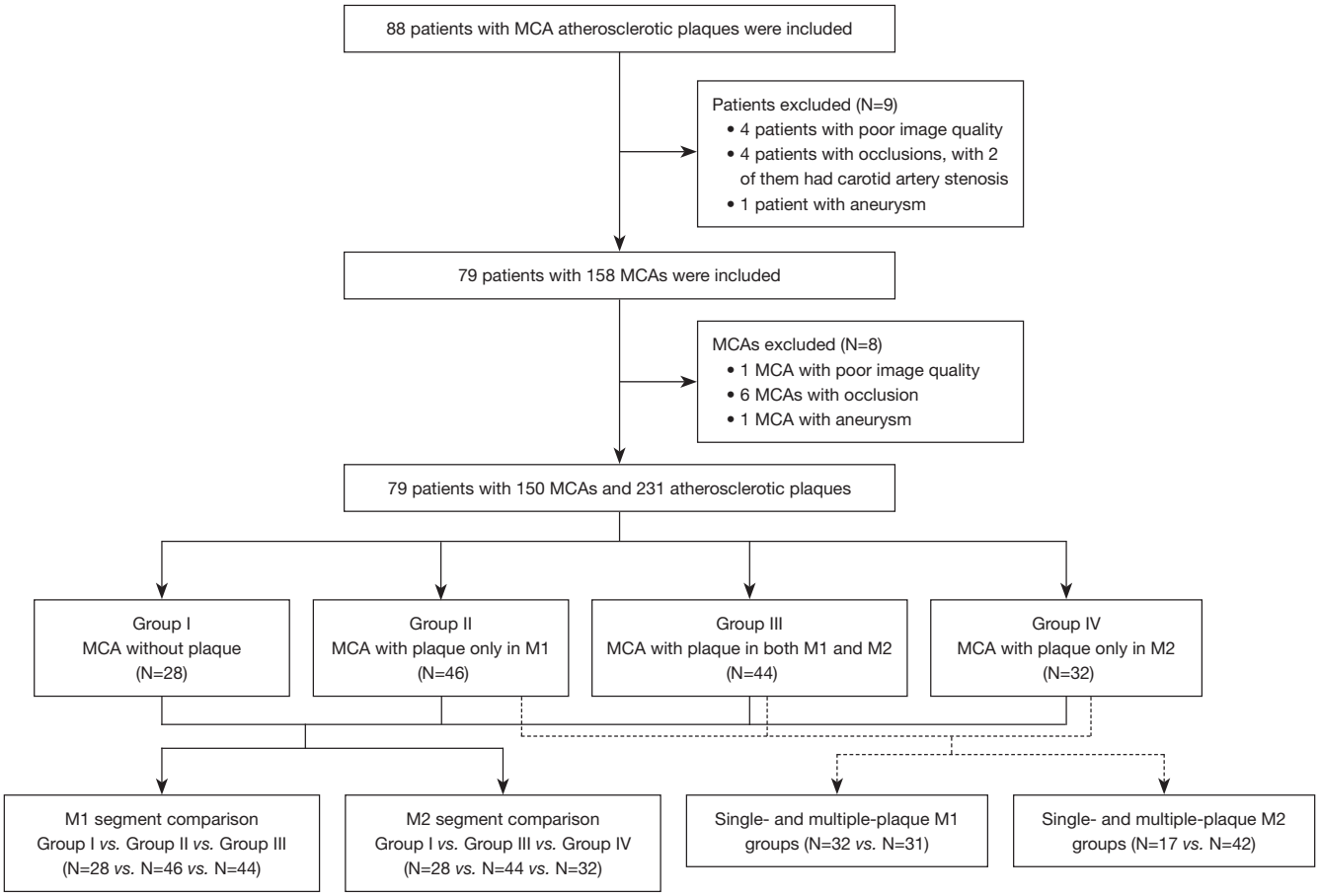

Figure 2 The flowchart of patient enrollment. MCA, middle cerebral artery.

Statistical analysis

All data were analyzed using SPSS 23.0 (IBM Corp., Armonk, NY, USA). The inter- and intra-observer agreements as well as scan-rescan MRIs of plaque characteristics and hemodynamic parameters were evaluated with the intraclass correlation coefficient (ICC): 0.00–0.20, poor correlation; 0.21–0.40, fair correlation; 0.41–0.60, moderate correlation; 0.61–0.80, good correlation; and 0.81–1.00, excellent correlation. All continuous variables were expressed as median (interquartile range) according to the Shapiro-Wilk test. Categorical variables were expressed as counts and percentages. Three-group comparisons of hemodynamic parameters in M1 and M2 plaque existence were evaluated using Kruskal-Wallis tests and post-hoc tests with Bonferroni correction. Geometric and plaque characteristics as well as hemodynamic parameters were compared between the single-plaque and multiple-plaque MCAs using Mann-Whitney *U* test. The categorical variables of these groups were analyzed through Chi-squared test or Fisher exact test. A two-sided $P<0.05$ was considered statistically significant.

Results

Demographic characteristics

Patient recruitment is shown in *Figure 2*. A total of 88 patients were initially recruited, of whom nine patients were excluded (poor image quality, N=4; occlusions of MCAs, including two carotid artery stenosis, N=4; aneurysm, N=1). Afterwards, in single MCA evaluation, eight MCAs were later excluded (poor image quality, N=1; occlusions of MCA, N=6; aneurysm, N=1). Overall, 150 MCAs of 79 patients were enrolled (median, 65 years; 56 males), with 231 atherosclerotic plaques identified on the 122 MCAs and 28 normal MCAs. According to plaque existence in different segments of MCA, the 150 MCAs

Table 2 Demographic information of patients

Characteristics	Values
Patient characteristics (N=79)	
Age (years)	65 [57–73]
Male	56 (70.89)
BMI (kg/m^2)	24.21 [22.43–26.51]
SBP (mmHg)	158 [140–172]
DBP (mmHg)	84 [77–95]
Cardiovascular risk factors	
Current smoking	28 (35.44)
Hyperlipidemia	34 (43.04)
Hypertension	67 (84.81)
Diabetes mellitus	38 (48.10)
Coronary disease	5 (6.33)
Prior stroke/TIA	9 (11.39)
Medication	
Statin	79 (100.00)
Antiplatelet	77 (97.47)
Collateral circulation improvement agent	79 (100.00)
NIHSS score at admission	3 [2–5]
0–5	62 (78.48)
>5	17 (21.52)
NIHSS score at discharge	2 [1–4]
0–5	67 (84.81)
>5	12 (15.19)
Plaque identification (N=150)	
MCA with plaque	122
With plaque only in M1	46
With plaque in both M1 and M2	44
With plaque only in M2	32
MCA without plaque	28

Values are presented as median [interquartile range], number (%) or number. BMI, body mass index; DBP, diastolic blood pressure; MCA, middle cerebral artery; NIHSS, National Institute of Health stroke scale; SBP, systolic blood pressure; TIA, transient ischemic stroke.

consisted of four parts: (I) without plaque (N=28); (II) with plaque only in M1 (N=46); (III) with plaque in both M1 and M2 (N=44); and (IV) with plaque only in M2 (N=32). The demographic characteristics of the 79 patients are shown in *Table 2*. Comparisons of WSS parameters in M1 (Groups I, II, and III) and M2 (Groups I, III, and IV) plaque existence are shown in *Tables 3*,*4* and Tables S1,S2. The single-plaque M1 group involved only the M1 with a single plaque of Group II (N=32), whereas the multiple-plaque M1 group (N=31) involved both the M1 with multiple plaques of Group II (N=14) as well as MCAs with the most stenotic plaque located in M1 of Group III (N=17). Similarly, the single-plaque M2 group involved only the M2 with a single plaque of Group IV (N=17), whereas the multiple-plaque M2 group (N=42) involved both the M2 with multiple plaques of Group IV (N=15) as well as MCAs with the most stenotic plaque located in M2 of Group III (N=27). The comparisons of geometric, plaque, and hemodynamic characteristics between single- and multiple-plaque MCAs are shown in *Table 5* and Table S3. According to ICC, good to excellent intra- and inter-reader agreement was obtained for all measurements of plaque characteristics (ICC >0.85; ICC >0.75), TAWSS (ICC >0.85; ICC >0.85), and OSI (ICC >0.75; ICC >0.75). As for scan-rescan tests, wall characteristics of maxWT and WA as well as TAWSS and OSI all showed excellent repeatability with ICC >0.80.

Hemodynamic alterations in the MCAs with and without plaque

$TAWSS_{min}$ showed a relatively larger value at the proximal portion compared to the distal portion across plaque in both M1 and M2 segments (Groups II, III, and IV). The post-hoc tests showed significant lower $TAWSS_{min}$ of Group III compared to Group II at the downstream slice (P=0.014) and Group III compared to Group I at the terminal slice (P=0.026) of M1 segment as well as Group IV compared to Group I at the upstream slice (P=0.008) and Group III compared to Group I at the terminal slice (P=0.010) of M2 segment. The value of $TAWSS_{min}$ was lower in Group II compared to Group I at the downstream and terminal slices, although the difference was not statistically significant. The lower segment-level $TAWSS_{min}$ of Group III compared to Group I was only found in M2 segment (P=0.039). Higher $TAWSS_{max}$ was only found in Group III compared to Group I at the initial slice (P=0.040) of M2 segment (Table S2). In addition, higher TAWSSCV was only found in Group IV compared to Group I at the upstream slice (P=0.043) of M2 segment (Table S2). Lower OSI_{mean} and OSI_{max} were found both in Group II compared to Group I of M1 segment (P=0.013 and P=0.036) at upstream slice and lower OSI_{mean}

Table 3 Hemodynamics of M1 segment in the MCAs with and without plaque

Parameters	Group I (N=28)	Group II (N=46)	Group III (N=44)	P values						
				I *vs.* II *vs.* III	I *vs.* II		I *vs.* III		II *vs.* III	
					Original	Adjusted†	Original	Adjusted†	Original	Adjusted†
Lesion-level WSS parameters										
$TAWSS_{min}$ (Pa)	1.77 (1.38–2.27)									
Initial		1.66 (1.01–2.26)	1.56 (1.01–2.50)	0.774						
Upstream		1.74 (1.04–2.61)	1.59 (0.97–2.77)	0.946						
MNL		2.26 (1.02–3.30)	1.55 (0.98–2.74)	0.363						
Downstream		1.74 (1.18–3.08)	1.22 (0.76–2.00)	0.009*	0.906	>0.999	0.019*	0.057	0.005*	0.014*
Terminal		1.37 (0.91–2.61)	1.03 (0.67–2.24)	0.025*	0.282	0.846	0.009*	0.026*	0.074	0.221
OSI_{mean}	0.020 (0.014–0.032)									
Initial		0.010 (0.004–0.022)	0.021 (0.006–0.033)	0.032*	0.010*	0.029*	0.194	0.582	0.145	0.436
Upstream		0.010 (0.003–0.030)	0.012 (0.005–0.023)	0.012*	0.004*	0.013*	0.016*	0.048*	0.623	>0.999
MNL		0.010 (0.004–0.041)	0.012 (0.004–0.025)	0.058						
Downstream		0.015 (0.004–0.036)	0.018 (0.006–0.039)	0.444						
Terminal		0.017 (0.005–0.044)	0.016 (0.006–0.040)	0.729						
Segment-level WSS parameters										
$TAWSS_{min}$ (Pa)	1.77 (1.38–2.27)	1.82 (1.39–2.38)	1.70 (1.24–2.07)	0.422						
OSI_{mean}	0.020 (0.014–0.032)	0.022 (0.012–0.035)	0.020 (0.012–0.032)	0.977						

Values are presented as median (interquartile range). Group I: MCA without plaque; Group II: MCA with plaque only in M1; Group III: MCA with plaque in both M1 and M2. In segments with multiple plaques, the most stenotic plaque was used in calculating plaque characteristics and lesion-level hemodynamics. In Group I, segment-level WSS-derived parameters were used as lesion-level hemodynamic parameters. †, P values were adjusted with Bonferroni correction. *, P<0.05. MCA, middle cerebral artery; MNL, the most narrowed lumen; OSI, oscillatory shear index; TAWSS, time-averaged wall shear stress; WSS, wall shear stress.

was also found in Group II compared to Group I of M1 segment (P=0.029) at initial slice and Group III compared to Group I of M1 segment (P=0.048) at the upstream slice (*Table 3* and Table S1). Other WSS-derived parameters showed no significant differences. Plaque location and hemodynamic characteristics of MCAs with and without plaque are shown in *Figure 3*.

Comparison of hemodynamics between single- and multiple-plaque MCAs

Lower lesion-level highest/initial $TAWSS_{mean}$ ratio

Table 4 Hemodynamics of M2 segment in the MCAs with and without plaque

Parameters	Group I (N=28)	Group III (N=44)	Group IV (N=32)	P values						
				I *vs.* III *vs.* IV	I *vs.* III		I *vs.* IV		III *vs.* IV	
					Original	Adjusted†	Original	Adjusted†	Original	Adjusted†
Lesion-level WSS parameters										
$TAWSS_{min}$ (Pa)	1.86 (1.65–2.18)									
Initial		1.32 (0.93–2.33)	1.96 (1.16–3.13)	0.042*	0.028*	0.085	0.816	>0.999	0.043*	0.130
Upstream		1.34 (0.83–2.40)	1.17 (0.84–1.80)	0.009*	0.026*	0.079	0.003*	0.008*	0.298	0.984
MNL		1.73 (0.88–2.59)	1.29 (0.88–3.02)	0.703						
Downstream		1.27 (0.81–2.17)	1.52 (0.77–2.58)	0.050						
Terminal		1.21 (0.80–2.01)	1.47 (0.89–2.72)	0.013*	0.003*	0.010*	0.140	0.421	0.157	0.472
OSI_{mean}	0.014 (0.010–0.033)									
Initial		0.017 (0.004–0.034)	0.008 (0.003–0.018)	0.054						
Upstream		0.011 (0.004–0.031)	0.012 (0.006–0.025)	0.158						
MNL		0.015 (0.005–0.025)	0.013 (0.003–0.033)	0.357						
Downstream		0.015 (0.005–0.025)	0.010 (0.003–0.037)	0.236						
Terminal		0.012 (0.004–0.025)	0.011 (0.003–0.042)	0.208						
Segment-level WSS parameters										
$TAWSS_{min}$ (Pa)	1.86 (1.65–2.18)	1.56 (1.28–2.02)	1.55 (1.33–2.19)	0.032*	0.013*	0.039*	0.036*	0.107	0.806	>0.999
OSI_{mean}	0.014 (0.010–0.033)	0.022 (0.011–0.037)	0.022 (0.011–0.031)	0.560						

Values are presented median (interquartile range). Group I: MCA without plaque; Group III: MCA with plaque in both M1 and M2; Group IV: MCA with plaque only in M2. In segments with multiple plaques, the most stenotic plaque was used in calculating plaque characteristics and lesion-level hemodynamics. In Group I, segment-level WSS-derived parameters were used as lesion-level hemodynamic parameters. †, P values were adjusted with Bonferroni correction. *, P<0.05. MCA, middle cerebral artery; MNL, the most narrowed lumen; OSI, oscillatory shear index; TAWSS, time-averaged wall shear stress; WSS, wall shear stress.

(P=0.037) and highest/initial $TAWSS_{max}$ ratio (P=0.013) were found in the single-plaque M1 group compared to the multiple-plaque M1 group (Table S3). A similar difference was not observed for the M2 segment. No significant differences in segment-level and other lesion-level WSS-derived parameters were found between single- and multiple-plaque groups.

Comparison of geometric and plaque characteristics between single- and multiple-plaque MCAs

The M1 geometry was different (P=0.027) between single-

Table 5 Comparison of geometric, plaque and hemodynamic characteristics between single- and multiple-plaque MCAs

Parameters	M1 group			M2 group		
	Single-plaque (N=32)	Multiple-plaque (N=31)	P value	Single-plaque (N=17)	Multiple-plaque (N=42)	P value
Geometric characteristics						
M1 geometry			0.027*			0.854
C type	20 (62.50)	23 (74.19)		15 (88.24)	33 (78.57)	
S type	11 (34.38)	3 (9.68)		–	2 (4.76)	
L type	1 (3.13)	5 (16.13)		2 (11.76)	7 (16.67)	
Plaque location			0.311			0.592
Proximal	8 (25.00)	12 (38.71)		8 (47.06)	23 (54.76)	
Middle	15 (46.88)	9 (29.03)		–	–	
Distal	9 (28.13)	10 (32.26)		9 (52.94)	19 (45.24)	
Plaque characteristics						
Plaque length (mm)	4.17 (2.73–8.36)	4.29 (3.28–7.12)	0.826	3.94 (2.48–7.17)	5.82 (2.54–10.85)	0.222
MaxWT (mm)	2.06 (1.66–2.52)	1.97 (1.74–2.29)	0.967	1.77 (1.53–2.15)	2.15 (1.86–2.45)	0.008*
WA (mm^2)	14.00 (10.26–16.43)	13.20 (11.04–15.04)	0.500	11.44 (8.58–14.12)	12.28 (11.24–15.19)	0.057
NWI	0.74 (0.69–0.79)	0.75 (0.71–0.82)	0.237	0.74 (0.69–0.79)	0.81 (0.75–0.90)	0.022*
RI	1.13 (0.98–1.28)	0.98 (0.86–1.12)	0.009*	0.99 (0.86–1.11)	0.99 (0.87–1.12)	0.867
Normal	5 (15.63)	6 (19.35)	0.041*	4 (23.53)	10 (23.81)	0.989
NR	6 (18.75)	14 (45.16)		7 (41.18)	18 (42.86)	
PR	21 (65.63)	11 (35.48)	0.017†*	6 (35.29)	14 (33.33)	0.885†
Degree of stenosis (%)	34.38 (8.54–55.00)	42.35 (28.71–62.18)	0.045*	37.97 (19.82–58.73)	52.63 (38.73–72.36)	0.049*
<50%	22 (68.75)	20 (64.52)	0.932	12 (70.59)	19 (45.24)	0.077
≥50%	10 (31.25)	11 (35.48)		5 (29.41)	23 (54.76)	
Lesion-level WSS parameters						
$TAWSS_{min}$ (Pa)						
Initial	1.70 (1.27–2.24)	1.24 (0.89–2.19)	0.254	2.06 (1.35–3.56)	1.34 (0.98–2.57)	0.076
Upstream	1.74 (1.03–2.38)	1.53 (0.82–3.26)	0.731	1.30 (0.92–2.14)	1.31 (0.85–2.61)	0.893
MNL	1.89 (0.88–2.92)	2.44 (1.10–3.94)	0.232	1.10 (0.89–3.02)	1.70 (0.81–3.33)	0.627
Downstream	1.86 (1.21–2.76)	1.59 (0.76–2.63)	0.290	1.50 (0.86–2.24)	1.30 (0.76–2.46)	0.947
Terminal	1.29 (0.87–2.50)	1.51 (0.79–2.54)	0.902	1.57 (1.03–3.08)	1.06 (0.73–2.25)	0.073
Lowest/initial $TAWSS_{min}$ ratio	0.65 (0.37–0.91)	0.66 (0.46–1.00)	0.719	0.44 (0.28–0.70)	0.53 (0.38–0.81)	0.155
MNL/REF $TAWSS_{min}$ ratio	1.10 (0.72–1.90)	1.56 (0.95–2.67)	0.221	0.93 (0.43–1.36)	1.16 (0.58–2.30)	0.197
OSI_{mean}						
Initial	0.010 (0.004–0.022)	0.017 (0.008–0.033)	0.182	0.009 (0.003–0.020)	0.008 (0.003–0.021)	0.987
Upstream	0.010 (0.004–0.028)	0.013 (0.003–0.023)	0.934	0.009 (0.007–0.018)	0.012 (0.004–0.031)	0.867
MNL	0.011 (0.004–0.042)	0.011 (0.003–0.017)	0.254	0.014 (0.004–0.032)	0.016 (0.004–0.030)	0.947
Downstream	0.015 (0.004–0.035)	0.015 (0.006–0.032)	0.912	0.011 (0.002–0.037)	0.014 (0.004–0.036)	0.422
Terminal	0.012 (0.005–0.044)	0.016 (0.005–0.045)	>0.999	0.012 (0.003–0.026)	0.015 (0.004–0.042)	0.323

Table 5 (*continued*)

Table 5 (*continued*)

Parameters	M1 group			M2 group		
	Single-plaque (N=32)	Multiple-plaque (N=31)	P value	Single-plaque (N=17)	Multiple-plaque (N=42)	P value
Segment-level WSS parameters						
$TAWSS_{min}$ (Pa)	1.76 (1.30–2.22)	1.86 (1.26–2.40)	0.837	1.65 (1.43–2.29)	1.51 (1.28–1.76)	0.132
OSI_{mean}	0.021 (0.012–0.034)	0.022 (0.011–0.033)	0.967	0.019 (0.010–0.029)	0.122 (0.090–0.158)	0.079

Values are presented as median (interquartile range) or number (%). In segments with multiple plaques, the most stenotic plaque was used in calculating plaque characteristics and lesion-level hemodynamics. †, comparisons were conducted between PR and non-PR group. *, P<0.05. MaxWT, maximum wall thickness; MCA, middle cerebral artery; MNL, the most narrowed lumen; NR, negative remodeling; NWI, normalized wall index; OSI, oscillatory shear index; PR, positive remodeling; REF, reference; RI, remodeling index; TAWSS, time-averaged wall shear stress; WA, wall area; WSS, wall shear stress.

and multiple-plaque M1 groups, with C type ranked the most frequently observed geometry in both groups followed by S type and L type in the single-plaque M1 group and L type and S type in the multiple-plaque M1 group. Geometry of the M1 segment showed no significant difference between the single- and multiple-plaque M2 groups. Meanwhile, the location of plaque was not significantly different between the single- and multiple-plaque groups.

Lower stenosis was observed in the single-plaque group compared to multiple-plaque groups (P=0.045 and P=0.049). Higher RI was only found in the single-plaque M1 group compared to the multiple-plaque M1 group (P=0.009) with more PR (21, 65.63% *vs.* 11, 35.48%, P=0.017). Compared with the multiple-plaque M2 group, the single-plaque M2 group exhibited lower maxWT (P=0.008) and NWI (P=0.022). Other plaque characteristics between the single- and multiple-plaque groups showed no significant differences.

Discussion

In this study, 4D flow and 3D T1W-VISTA were used for the combined evaluation of plaque characteristics and WSS parameters in different segments of MCA. Our results showed that there were plaque-related alterations of TAWSS and OSI in both M1 and M2 segments of MCA, and the pattern of the alterations differed between the two segments. Generally, plaque-related low lesion-level $TAWSS_{min}$ was observed in the M2 segment, whereas low lesion-level $TAWSS_{min}$ and OSI were observed in the M1 segment, although the results were heterogeneous regarding the level of significance and the slices. Segment-level lower $TAWSS_{min}$ was only observed in the presence of M2 plaque. In the comparisons between single- and multiple-plaque groups, lower lesion-level highest/initial $TAWSS_{mean}$ ratio and highest/initial $TAWSS_{max}$ ratio were only found in the single-plaque M1 group compared to the multiple-plaque M1 group. Lower stenosis was observed in the single-plaque group compared to the multiple-plaque group. Higher RI was only found in the single-plaque M1 group compared to the multiple-plaque M1 group, whereas lower maxWT and NWI were only seen in the single-plaque M2 group compared to the multiple-plaque M2 group.

Our result that the TAWSS was reduced in MCAs with atherosclerosis compared to MCAs without plaque was consistent with previous extracranial arterial studies (11-13,18,42-44). The similar results that low TAWSS favors the presence of plaque in aorta, coronary artery, carotid artery as well as intracranial artery further elucidated the interaction between WSS and atherosclerosis. The potential reason may be that the impacts of existing plaque could cause changes to local vessel geometry, which might alter regional hemodynamics. Although no significant difference was found in $TAWSS_{min}$ between MCAs with the presence of only M1 plaque and nonplaque MCAs in the current study, the lower value of $TAWSS_{min}$ in the downstream and terminal slices of atherosclerotic M1 also indicated the potential for a similar trend and that the relationship could be significant if a larger sample size and more severe stenotic plaque were included. In addition, the segment-level lower $TAWSS_{min}$ observed only in the M2 segment may be due to the possible explanation that the total length of the M1 segment is much longer than the plaque length and local flow alterations caused by plaque could be remedied through normal sections and cerebral vascular autoregulation. In the present study, TAWSSCV was calculated to determine the spatial change of WSS in values, and higher $TWASS_{max}$ and TAWSSCV were only observed in the presence of

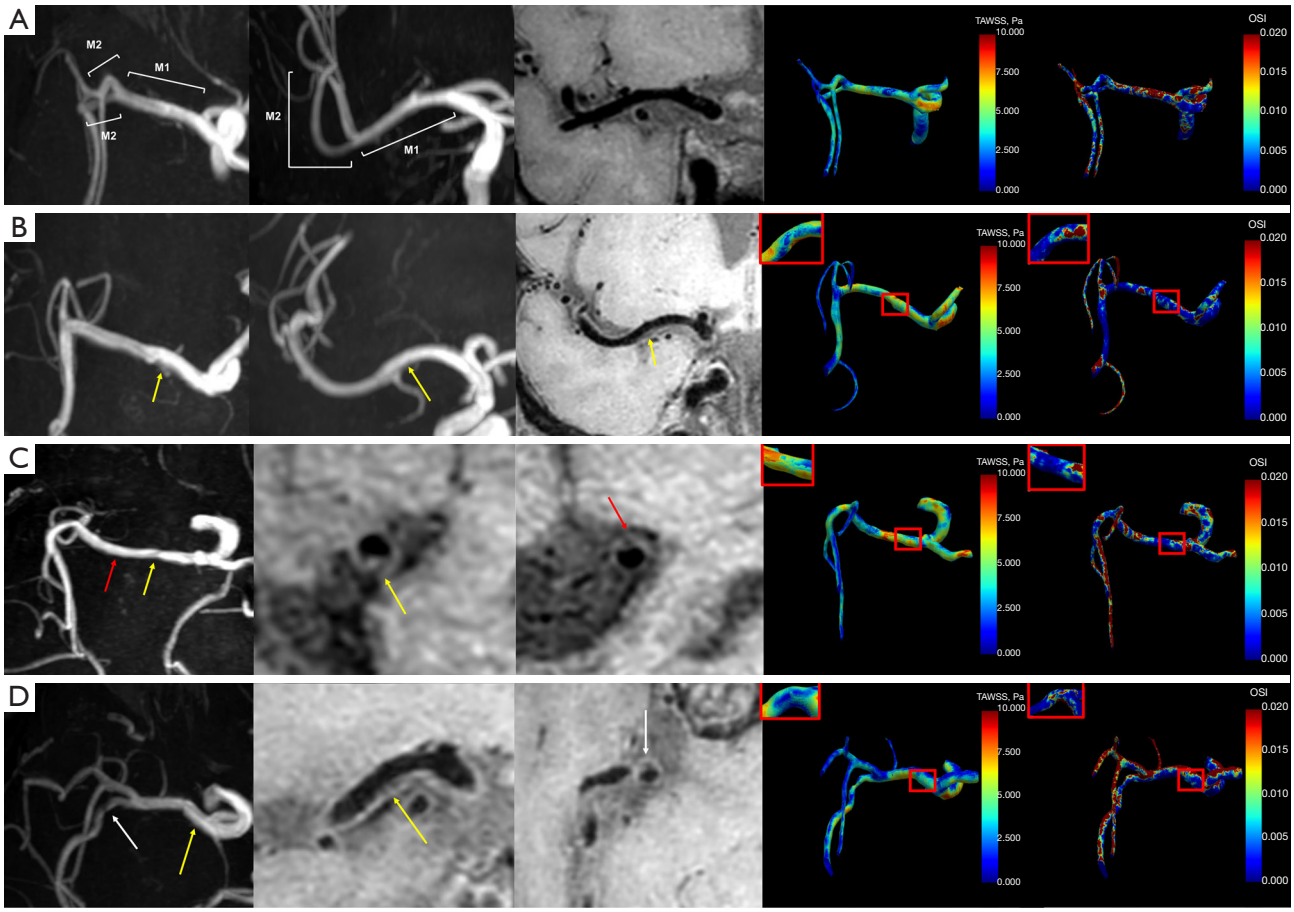

Figure 3 Plaque location and hemodynamic characteristics of MCAs with and without plaque. (A) A right MCA without plaque. Left to right, axial and coronal MIP images of 3D TOF MRA, a coronal MPR image of 3D HR-VWI and maps of TAWSS and OSI distributions. White brackets show the M1 and M2 segments. (B) A right atherosclerotic MCA with a single plaque in M1. Left to right, axial and coronal MIP images of 3D TOF MRA, a coronal MPR image of 3D HR-VWI and maps of TAWSS and OSI distributions. Yellow arrow shows the location of the plaque. (C) A right atherosclerotic MCA with multiple plaques in M1 (N=2). Left to right, an MIP images of 3D TOF MRA, cross-sectional images of 3D HR-VWI and maps of TAWSS and OSI distributions. Yellow and red arrows respectively show the locations of the plaques while yellow one indicated the most stenotic plaque. (D) A right atherosclerotic MCA with plaques in both M1 and M2. Left to right, an MIP images of 3D TOF MRA, cross-sectional images of 3D HR-VWI and maps of TAWSS and OSI distributions. Yellow and white arrows respectively show the locations of the most stenotic plaques in M1 and M2 segments. The red boxes in the distribution maps indicate the regional TAWSS and OSI of M1 plaques (yellow arrows). The red boxes in the upper right corner show the maps of regional TAWSS and OSI in different orientations. 3D, three-dimensional; HR-VWI, high-resolution vessel wall imaging; MCA, middle cerebral artery; MIP, maximum intensity projection; MNL, the most narrowed lumen; MPR, multiplanar reformation; MRA, magnetic resonance angiography; OSI, oscillatory shear index; TAWSS, time-averaged wall shear stress; TOF, time-of-flight.

M2 plaque, which suggested a wider range of unevenly distributed TAWSS values and reflected regional unstable flow since M2 branches exhibited more complex morphology than M1 segment and the small LA of M2 segment may be more sensitive to the influence of plaque.

As for the lower OSI observed in the MCAs with plaque compared to MCAs without plaque in the present study, the result was in line with some studies (11,18,19) but in contrast to others (9,15,17). A previous CFD cross-sectional study of healthy subjects indicated no relation between OSI and carotid intima-medial thickness (45). Meanwhile, a 4D flow study found no significant difference of OSI distribution between carotid atherosclerosis and healthy subjects (46). Another 4D flow analysis demonstrated a good

correlation between low WSS but not high OSI with plaque distribution between aortic atherosclerosis and healthy volunteers (11). On the contrary, other studies revealed high OSI in the presence of atherosclerosis (9,15,17). Studies related to aneurysms also indicated the associations of low TAWSS and high OSI with tissue degradation (47,48) which may also play a role in the progression of atherosclerosis. In a baseline and 6-month follow-up study of coronary atherosclerosis, different roles of oscillatory and non-oscillatory WSS with plaque progression were both observed (18). They indicated that plaque with oscillatory WSS exhibited total plaque as well as fibrous tissue regression towards a more vulnerable phenotype whereas plaque displaying non-oscillatory WSS showed total plaque progression towards a more stable lesion with accumulation of total plaque and fibrous tissue area (18). Moreover, a recent study investigating the relation of hemodynamics and plaque vulnerability features found that unlike the general assumption, low OSI areas did not always coincide with high TAWSS (19). They revealed a significantly larger cap thickness in areas exposed to both low TAWSS and low OSI (19). In addition, the current control (i.e., MCAs without plaque) is not derived from straight blood vessels, and some planes stay close to the bifurcations (internal carotid artery-M1/A1 or M1-M2) or within the curved part of M1 and/or M2 segments, so the blood flow may be affected, which may lead to a higher OSI; however, we used segment-level hemodynamics to reduce the potential influence of vessel geometry. Therefore, the OSI result found in our study could occur and be different in slices or segments according to the location of plaque and the interplay between existing plaque and local flow changes.

The comparisons between single- and multiple-plaque groups in the current study suggested the influences of plaque number on existing atherosclerosis and hemodynamics. Previous studies have discovered that plaque number could be a potential risk factor of IS prognosis (23-26) and the overall alterations of corresponding flow conditions could be influenced by the presence of each plaque in the entire vascular territory. The lower lesion-level highest/initial $TAWSS_{mean}$ ratio and highest/initial $TAWSS_{max}$ observed in the single-plaque M1 group compared to the multiple-plaque M1 group suggested fluctuation of local TAWSS and reflected the potential influence of other plaque on the most stenotic one of multiple-plaques. Higher WSS spatial gradient within plaque implicated potential instability (49) and increased risk for IS occurrence (5). The reason that the above flow changes were not seen in the M2 segment may be attributed to the congenital anatomy variations of M1 and M2 segments as well as the presence of plaque. However, we did not find a significant difference in $TAWSS_{min}$ between single- and multiple-plaque groups. The elevated WSS or WSS gradient which accompanied the unfavorable prognosis (5,18,49) could be the possible explanation.

In addition, our study demonstrated that a single plaque in M1 is more likely to have PR, whereas a single plaque in M2 may have a lighter plaque burden than the multiple-plaque counterpart. Vascular remodeling is a compensatory phenomenon that occurs in arterial walls during the initiation and progression of atherosclerotic lesions (20,50). The PR causes vessel enlargement and alleviates vessel stenosis to some extent, while the NR results in constriction of the LA. The remodeling patterns of local atherosclerosis can be constant or altered in the evolution of atherosclerosis (20,50,51). Therefore, the lumen preservation due to compensatory or excessive expansive remodeling and the lumen constriction due to constrictive remodeling can be dynamic in different stages of plaque development. The PR in our study was more of a compensatory reaction of the vessel due to relatively mild stenosis instead of excessive expansive remodeling (52). Moreover, lower stenosis seen in the single-plaque group compared to multiple-plaque groups also facilitate the explanation.

In the current study, multiple comparisons were conducted to discover potential flow changing markers (i.e., WSS-derived parameters) in the presence of plaque and in single- and multiple-plaque MCAs. The post-hoc tests with Bonferroni correction were used for adjustments in hemodynamic comparisons in the presence of MCA plaque of different segments. We did not include rigorous adjustments because of the inclusions of both MCAs of patients and simple comparison of the clinical factors could have incurred bias. In future research, we will explore this further by including more cases and subgroups.

The strength of this study is that both lesion- and segment-level TAWSS and OSI were measured and compared between different plaque subgroups, providing a comprehensive insight into the interplay between existing plaque and hemodynamics. The application of 4D flow and 3D VWI enables both assessment of real-world intracranial hemodynamics and accurate measurement of plaque characteristics. The findings not only verify plaque existence, location, and numbers on regional hemodynamics, but also expand the application of these associations in mild stenosis and M2 segments, which

previous studies have rarely investigated.

This study has several limitations. Firstly, it was a single-center study with a small sample size. Further validation of the regional hemodynamics needs to be conducted through a multi-center study with a larger sample size. Secondly, this was a cross-sectional study, the causal relationship between specific flow alteration and plaques formation is quite impossible to assess without follow-up scanning. Thirdly, the number of patients with a severe disability such as with moderate-to-high stenosis (i.e., ≥50%) was relatively small. This may affect the statistical power in comparing between groups in this study. Fourthly, symptomatic and asymptomatic plaques were not compared in the current study, so as the roles of hemodynamic changes in the transition from asymptomatic to culprit plaque cannot be assessed. Fifthly, we separated the single-plaque group from the multiple-plaque group only based on the total plaque number of the entire MCA. Future studies with larger sample size may further explore the potential influences of co-existing atherosclerosis between M1 and M2 segments as well as the potential different hemodynamics between tandem and parallel plaques of M2 segments. Sixthly, hemodynamics such as pressure change (53,54) and phase shift (55) between pressure and WSS (or velocity) are closely related to atherosclerosis (56). However, due to technical limitations (54) we were unable to calculate these parameters. Future studies of atherosclerosis may benefit by including these flow parameters. Finally, this study did not include post-contrast VWI to evaluate intracranial atherosclerotic enhancement which is important in the differentiation of plaque vulnerability and measurements of local hemodynamic alterations. Therefore, the information that this study can provide on the association of flow parameters and plaque vulnerability is very limited. Studies including both pre- and post-contrast MRI would be helpful to further facilitate the identification associations between hemodynamics and high-risk atherosclerosis.

Conclusions

The presence of plaque could cause alterations of hemodynamics and these flow patterns may be different between M1 plaque and M2 plaque. Different geometry, plaque characteristics, and hemodynamics were observed in the comparisons between single- and multiple-plaque MCAs of different segments. These findings might serve to further reveal the mechanisms of intracranial atherosclerotic existence.

Acknowledgments

None.

Footnote

Reporting Checklist: The authors have completed the STROBE reporting checklist. Available at https://qims.amegroups.com/article/view/10.21037/qims-24-1733/rc

Funding: This work was supported by the Guiding Project of Department of Science and Technology of Fujian Province (No. 2021Y0017 to P.J.), the Natural Science Foundation of Shanghai (No. 22ZR1403900 to Z.C.), and the National Natural Science Foundation of China (No. 82302156 to Z.C.).

Conflicts of Interest: All authors have completed the ICMJE uniform disclosure form (available at https://qims.amegroups.com/article/view/10.21037/qims-24-1733/coif). The authors have no conflicts of interest to declare.

Ethical Statement: The authors are accountable for all aspects of the work in ensuring that questions related to the accuracy or integrity of any part of the work are appropriately investigated and resolved. This study was conducted in accordance with the Declaration of Helsinki (as revised in 2013) and was approved by the Ethics Committee of Fujian Medical University Union Hospital (No. 2021KJT066). Written informed consent was provided by each patient.

References

1. Yao W, Chen H, Huang K, Peng W, Zhang X, Yang D, Teng Z, Shen J, Yang J, Cheng X, Han Y, Zhu W, Wang J, Du J, Liu X. Atherosclerotic plaque evolution predicts cerebral ischemic events in patients with intracranial

atherosclerosis: a multicentre longitudinal study using high-resolution MRI. Eur Radiol 2024. [Epub ahead of print]. doi: 10.1007/s00330-024-11248-8.
2. Xu WH, Li ML, Gao S, Ni J, Zhou LX, Yao M, Peng B, Feng F, Jin ZY, Cui LY. In vivo high-resolution MR imaging of symptomatic and asymptomatic middle cerebral artery atherosclerotic stenosis. Atherosclerosis 2010;212:507-11.
3. Pu Y, Lan L, Leng X, Wong LK, Liu L. Intracranial atherosclerosis: From anatomy to pathophysiology. Int J Stroke 2017;12:236-45.
4. Liu Y, Li S, Liu H, Tian X, Liu Y, Li Z, Leung TW, Leng X. Clinical implications of haemodynamics in symptomatic intracranial atherosclerotic stenosis by computational fluid dynamics modelling: a systematic review. Stroke Vasc Neurol 2025;10:16-24.
5. Woo HG, Kim HG, Lee KM, Ha SH, Jo H, Heo SH, Chang DI, Liebeskind DS, Kim BJ. Wall Shear Stress Associated with Stroke Occurrence and Mechanisms in Middle Cerebral Artery Atherosclerosis. J Stroke 2023;25:132-40.
6. Slager CJ, Wentzel JJ, Gijsen FJ, Schuurbiers JC, van der Wal AC, van der Steen AF, Serruys PW. The role of shear stress in the generation of rupture-prone vulnerable plaques. Nat Clin Pract Cardiovasc Med 2005;2:401-7.
7. Cecchi E, Giglioli C, Valente S, Lazzeri C, Gensini GF, Abbate R, Mannini L. Role of hemodynamic shear stress in cardiovascular disease. Atherosclerosis 2011;214:249-56.
8. Bai X, Fu M, Li Z, Gao P, Zhao H, Li R, Sui B. Distribution and regional variation of wall shear stress in the curved middle cerebral artery using four-dimensional flow magnetic resonance imaging. Quant Imaging Med Surg 2022;12:5462-73.
9. Markl M, Wegent F, Zech T, Bauer S, Strecker C, Schumacher M, Weiller C, Hennig J, Harloff A. In vivo wall shear stress distribution in the carotid artery: effect of bifurcation geometry, internal carotid artery stenosis, and recanalization therapy. Circ Cardiovasc Imaging 2010;3:647-55.
10. Zhou M, Yu Y, Chen R, Liu X, Hu Y, Ma Z, Gao L, Jian W, Wang L. Wall shear stress and its role in atherosclerosis. Front Cardiovasc Med 2023;10:1083547.
11. Harloff A, Nussbaumer A, Bauer S, Stalder AF, Frydrychowicz A, Weiller C, Hennig J, Markl M. In vivo assessment of wall shear stress in the atherosclerotic aorta using flow-sensitive 4D MRI. Magn Reson Med 2010;63:1529-36.
12. Suo J, Oshinski JN, Giddens DP. Blood flow patterns in the proximal human coronary arteries: relationship to atherosclerotic plaque occurrence. Mol Cell Biomech 2008;5:9-18.
13. Han N, Wang J, Ma Y, Ma L, Zheng Y, Fan F, Wu C, Yue S, Li J, Liang J, Zhang H, Zhou Y, Yang T, Zhang J. The hemodynamic and geometric characteristics of carotid artery atherosclerotic plaque formation. Quant Imaging Med Surg 2024;14:4348-61.
14. Peiffer V, Sherwin SJ, Weinberg PD. Does low and oscillatory wall shear stress correlate spatially with early atherosclerosis? A systematic review. Cardiovasc Res 2013;99:242-50.
15. Steinman DA, Thomas JB, Ladak HM, Milner JS, Rutt BK, Spence JD. Reconstruction of carotid bifurcation hemodynamics and wall thickness using computational fluid dynamics and MRI. Magn Reson Med 2002;47:149-59.
16. Olgac U, Poulikakos D, Saur SC, Alkadhi H, Kurtcuoglu V. Patient-specific three-dimensional simulation of LDL accumulation in a human left coronary artery in its healthy and atherosclerotic states. Am J Physiol Heart Circ Physiol 2009;296:H1969-82.
17. Hoi Y, Zhou YQ, Zhang X, Henkelman RM, Steinman DA. Correlation between local hemodynamics and lesion distribution in a novel aortic regurgitation murine model of atherosclerosis. Ann Biomed Eng 2011;39:1414-22.
18. Timmins LH, Molony DS, Eshtehardi P, McDaniel MC, Oshinski JN, Giddens DP, Samady H. Oscillatory wall shear stress is a dominant flow characteristic affecting lesion progression patterns and plaque vulnerability in patients with coronary artery disease. J R Soc Interface 2017;14:20160972.
19. Moerman AM, Korteland S, Dilba K, van Gaalen K, Poot DHJ, van Der Lugt A, Verhagen HJM, Wentzel JJ, van Der Steen AFW, Gijsen FJH, Van der Heiden K. The Correlation Between Wall Shear Stress and Plaque Composition in Advanced Human Carotid Atherosclerosis. Front Bioeng Biotechnol 2021;9:828577.
20. Koskinas KC, Feldman CL, Chatzizisis YS, Coskun AU, Jonas M, Maynard C, Baker AB, Papafaklis MI, Edelman ER, Stone PH. Natural history of experimental coronary atherosclerosis and vascular remodeling in relation to endothelial shear stress: a serial, in vivo intravascular ultrasound study. Circulation 2010;121:2092-101.
21. Wentzel JJ, Chatzizisis YS, Gijsen FJ, Giannoglou GD, Feldman CL, Stone PH. Endothelial shear stress in the evolution of coronary atherosclerotic plaque and vascular remodelling: current understanding and remaining questions. Cardiovasc Res 2012;96:234-43.

22. Wang J, Paritala PK, Mendieta JB, Gu Y, Raffel OC, McGahan T, Lloyd T, Li Z. Carotid Bifurcation With Tandem Stenosis-A Patient-Specific Case Study Combined in vivo Imaging, in vitro Histology and in silico Simulation. Front Bioeng Biotechnol 2019;7:349.
23. Wu G, Wang H, Zhao C, Cao C, Chai C, Huang L, Guo Y, Gong Z, Tirschwell DL, Zhu C, Xia S. Large Culprit Plaque and More Intracranial Plaques Are Associated with Recurrent Stroke: A Case-Control Study Using Vessel Wall Imaging. AJNR Am J Neuroradiol 2022;43:207-15.
24. Sun B, Wang L, Li X, Zhang J, Zhang J, Liu X, Wu H, Mossa-Basha M, Xu J, Zhao B, Zhao H, Zhou Y, Zhu C. Intracranial Atherosclerotic Plaque Characteristics and Burden Associated With Recurrent Acute Stroke: A 3D Quantitative Vessel Wall MRI Study. Front Aging Neurosci 2021;13:706544.
25. Xu Y, Yuan C, Zhou Z, He L, Mi D, Li R, Cui Y, Wang Y, Wang Y, Liu G, Zheng Z, Zhao X. Co-existing intracranial and extracranial carotid artery atherosclerotic plaques and recurrent stroke risk: a three-dimensional multicontrast cardiovascular magnetic resonance study. J Cardiovasc Magn Reson 2016;18:90.
26. Fernández-Friera L, García-Alvarez A, Oliva B, García-Lunar I, García I, Moreno-Arciniegas A, Gómez-Talavera S, Pérez-Herreras C, Sánchez-González J, de Vega VM, Rossello X, Bueno H, Fernández-Ortiz A, Ibañez B, Sanz J, Fuster V. Association between subclinical atherosclerosis burden and unrecognized myocardial infarction detected by cardiac magnetic resonance in middle-aged low-risk adults. Eur Heart J Cardiovasc Imaging 2024;25:968-75.
27. Tian X, Fang H, Lan L, Ip HL, Abrigo J, Liu H, Zheng L, Fan FSY, Ma SH, Ip B, Song B, Xu Y, Li J, Zhang B, Xu Y, Soo YOY, Mok V, Wong KS, Leung TW, Leng X. Risk stratification in symptomatic intracranial atherosclerotic disease with conventional vascular risk factors and cerebral haemodynamics. Stroke Vasc Neurol 2023;8:77-85.
28. Tian X, Shi Z, Wang Z, Xu B, Peng WJ, Zhang XF, Liu Q, Chen SY, Tian B, Lu JP, Shao CW. Characteristics of culprit intracranial plaque without substantial stenosis in ischemic stroke using three-dimensional high-resolution vessel wall magnetic resonance imaging. Front Neurosci 2023;17:1160018.
29. Wu XB, Liu YA, Huang LX, Guo X, Cai WQ, Luo B, Wang SW. Hemodynamics combined with inflammatory indicators exploring relationships between ischemic stroke and symptomatic middle cerebral artery atherosclerotic stenosis. Eur J Med Res 2023;28:378.
30. Chen Z, Qin H, Liu J, Wu B, Cheng Z, Jiang Y, Liu L, Jing L, Leng X, Jing J, Wang Y, Wang Y. Characteristics of Wall Shear Stress and Pressure of Intracranial Atherosclerosis Analyzed by a Computational Fluid Dynamics Model: A Pilot Study. Front Neurol 2019;10:1372.
31. Kasner SE, Chimowitz MI, Lynn MJ, Howlett-Smith H, Stern BJ, Hertzberg VS, Frankel MR, Levine SR, Chaturvedi S, Benesch CG, Sila CA, Jovin TG, Romano JG, Cloft HJ; . Predictors of ischemic stroke in the territory of a symptomatic intracranial arterial stenosis. Circulation 2006;113:555-63.
32. Malik J, Novakova L, Valerianova A, Chytilova E, Lejsek V, Buryskova Salajova K, Lambert L, Grus T, Porizka M, Michalek P. Wall Shear Stress Alteration: a Local Risk Factor of Atherosclerosis. Curr Atheroscler Rep 2022;24:143-51.
33. Lan L, Liu H, Ip V, Soo Y, Abrigo J, Fan F, Ma SH, Ma K, Ip B, Liu J, Fan Y, Zeng J, Mok V, Wong L, Liebeskind D, Leung T, Leng X. Regional High Wall Shear Stress Associated With Stenosis Regression in Symptomatic Intracranial Atherosclerotic Disease. Stroke 2020;51:3064-73.
34. Morgan AG, Thrippleton MJ, Wardlaw JM, Marshall I. 4D flow MRI for non-invasive measurement of blood flow in the brain: A systematic review. J Cereb Blood Flow Metab 2021;41:206-18.
35. Wåhlin A, Eklund A, Malm J. 4D flow MRI hemodynamic biomarkers for cerebrovascular diseases. J Intern Med 2022;291:115-27.
36. Turski P, Scarano A, Hartman E, Clark Z, Schubert T, Rivera L, Wu Y, Wieben O, Johnson K. Neurovascular 4DFlow MRI (Phase Contrast MRA): emerging clinical applications. Neurovascular Imaging 2016;2:8.
37. Qiao Y, Zeiler SR, Mirbagheri S, Leigh R, Urrutia V, Wityk R, Wasserman BA. Intracranial plaque enhancement in patients with cerebrovascular events on high-spatial-resolution MR images. Radiology 2014;271:534-42.
38. Chen Z, Liu AF, Chen H, Yuan C, He L, Zhu Y, Guan M, Jiang WJ, Zhao X. Evaluation of basilar artery atherosclerotic plaque distribution by 3D MR vessel wall imaging. J Magn Reson Imaging 2016;44:1592-9.
39. Yu YN, Li ML, Xu YY, Meng Y, Trieu H, Villablanca JP, Gao S, Feng F, Liebeskind DS, Xu WH. Middle cerebral artery geometric features are associated with plaque distribution and stroke. Neurology 2018;91:e1760-9.
40. Han J, Qiao H, Li X, Li X, He Q, Wang Y, Cheng Z. The three-dimensional shape analysis of the M1 segment of the middle cerebral artery using MRA at 3T. Neuroradiology

2014;56:995-1005.
41. Petersson S, Dyverfeldt P, Ebbers T. Assessment of the accuracy of MRI wall shear stress estimation using numerical simulations. J Magn Reson Imaging 2012;36:128-38.
42. van der Giessen AG, Wentzel JJ, Meijboom WB, Mollet NR, van der Steen AF, van de Vosse FN, de Feyter PJ, Gijsen FJ. Plaque and shear stress distribution in human coronary bifurcations: a multislice computed tomography study. EuroIntervention 2009;4:654-61.
43. Tricot O, Mallat Z, Heymes C, Belmin J, Lesèche G, Tedgui A. Relation between endothelial cell apoptosis and blood flow direction in human atherosclerotic plaques. Circulation 2000;101:2450-3.
44. Slager CJ, Wentzel JJ, Gijsen FJ, Thury A, van der Wal AC, Schaar JA, Serruys PW. The role of shear stress in the destabilization of vulnerable plaques and related therapeutic implications. Nat Clin Pract Cardiovasc Med 2005;2:456-64.
45. Augst AD, Ariff B, McG Thom SA, Xu XY, Hughes AD. Analysis of complex flow and the relationship between blood pressure, wall shear stress, and intima-media thickness in the human carotid artery. Am J Physiol Heart Circ Physiol 2007;293:H1031-7.
46. El Sayed R, Park CC, Shah Z, Nahab FB, Haussen DC, Allen JW, Oshinski JN. Assessment of Complex Flow Patterns in Patients With Carotid Webs, Patients With Carotid Atherosclerosis, and Healthy Subjects Using 4D Flow MRI. J Magn Reson Imaging 2024;59:2001-10.
47. Wang H, Balzani D, Vedula V, Uhlmann K, Varnik F. On the Potential Self-Amplification of Aneurysms Due to Tissue Degradation and Blood Flow Revealed From FSI Simulations. Front Physiol 2021;12:785780.
48. Wang H, Uhlmann K, Vedula V, Balzani D, Varnik F. Fluid-structure interaction simulation of tissue degradation and its effects on intra-aneurysm hemodynamics. Biomech Model Mechanobiol 2022;21:671-83.
49. Dolan JM, Kolega J, Meng H. High wall shear stress and spatial gradients in vascular pathology: a review. Ann Biomed Eng 2013;41:1411-27.
50. Chatzizisis YS, Coskun AU, Jonas M, Edelman ER, Feldman CL, Stone PH. Role of endothelial shear stress in the natural history of coronary atherosclerosis and vascular remodeling: molecular, cellular, and vascular behavior. J Am Coll Cardiol 2007;49:2379-93.
51. Samady H, Eshtehardi P, McDaniel MC, Suo J, Dhawan SS, Maynard C, Timmins LH, Quyyumi AA, Giddens DP. Coronary artery wall shear stress is associated with progression and transformation of atherosclerotic plaque and arterial remodeling in patients with coronary artery disease. Circulation 2011;124:779-88.
52. Zhang D, Wu X, Tang J, Wang P, Chen GZ, Yin X. Hemodynamics is associated with vessel wall remodeling in patients with middle cerebral artery stenosis. Eur Radiol 2021;31:5234-42.
53. Bouaou K, Dietenbeck T, Soulat G, Bargiotas I, Houriez-Gombaud-Saintonge S, De Cesare A, Gencer U, Giron A, Jiménez E, Messas E, Lucor D, Bollache E, Mousseaux E, Kachenoura N. Four-dimensional flow cardiovascular magnetic resonance aortic cross-sectional pressure changes and their associations with flow patterns in health and ascending thoracic aortic aneurysm. J Cardiovasc Magn Reson 2024;26:101030.
54. Marlevi D, Schollenberger J, Aristova M, Ferdian E, Ma Y, Young AA, Edelman ER, Schnell S, Figueroa CA, Nordsletten DA. Noninvasive quantification of cerebrovascular pressure changes using 4D Flow MRI. Magn Reson Med 2021;86:3096-110.
55. Wang H, Krüger T, Varnik F. Geometry and flow properties affect the phase shift between pressure and shear stress waves in blood vessels. Fluids 2021;6:378.
56. Leng X, Wong KS, Liebeskind DS. Evaluating intracranial atherosclerosis rather than intracranial stenosis. Stroke 2014;45:645-51.

Cite this article as: Jiang P, Liu L, Qiao H, Xu X, Zheng Y, Lin L, Chen J, Sun B, Wang H, Zhao X, Chen Z, Xue Y. Anatomical location-related hemodynamic variations are associated with atherosclerosis in the middle cerebral artery: a preliminary cross-sectional 4D flow and 3D vessel wall MRI study. Quant Imaging Med Surg 2025;15(4):3585-3601. doi: 10.21037/qims-24-1733